Natural Convection Flow in a Strong Cross Magnetic Field with Radiation

S. Siddiqa
Assistant Professor
Department of Mathematics
COMSATS Institute of
Information Technology,
Kamra Road, Attock, Pakistan
Email: saadiasiddiqa@gmail.com

M. A. Hossain
Rtd. Professor
Department of Mathematics
University of Dhaka
Dhaka, Bangladesh
Email: anwar@univdhaka.edu

Suvash C. Saha*
Postdoctoral Research Fellow
School of Chemistry, Physics & Mechanical Engineering
Queensland University of Technology
GPO Box 2434, Brisbane Queensland 4001, Australia
Email: s_c_saha@yahoo.com, suvash.saha@qut.edu.au

ABSTRACT

The problem of MHD natural convection boundary layer flow of an electrically conducting and optically dense gray viscous fluid along a heated vertical plate is analyzed in the presence of strong cross magnetic field with radiative heat transfer. In the analysis radiative heat flux is considered by adopting optically thick radiation limit. Attempt is made to obtain the solutions valid for liquid metals by taking $Pr \ll 1$. *Boundary layer equations are transformed in to a con-*

*Address all correspondence to this author.

venient dimensionless form by using stream function formulation (SFF) and primitive variable formulation (PVF). Non-similar equations obtained from SFF are then simulated by implicit finite difference (Keller-box) method whereas parabolic partial differential equations obtained from PVF are integrated numerically by hiring direct finite difference method over the entire range of local Hartmann parameter, ξ. Further, asymptotic solutions are also obtained for large and small values of local Hartmann parameter ξ. A favorable agreement is found between the results for small, large and all values of ξ. Numerical results are also demonstrated graphically by showing the effect of various physical parameters on shear stress, rate of heat transfer, velocity and temperature.

Nomenclature

g Acceleration due to gravity.

c_p Specific heat at constant temperature.

Gr_x Grashof number.

Pr Prandtl number.

T Temperature of the fluid in the boundary layer.

T_∞ Temperature of the ambient fluid.

T_w Temperature at the surface.

u, v Dimensional fluid velocities in the x- and y- direction respectively.

$\bar{u}, \bar{v}$ Dimension less fluid velocities in the $\bar{x}$- and $\bar{y}$- direction respectively.

x, y Dimensional Cartesian coordinates.

$\bar{x}, \bar{y}$ Dimension less Cartesian coordinates.

a Rosseland mean absorption coefficient.

τ_w Dimensionless shear-stress.

q_r Radiative heat flux.

R_d Radiation parameter.

Q Dimensionless heat transfer.

B_0 Magnetic field.

ψ Stream function.

κ Thermal conductivity.

α Thermal diffusivity.

β Volumetric coefficient of thermal expansion.

μ Dynamical viscosity.

ν Kinematic viscosity.

θ Dimensionless temperature function.

θ_w Surface temperature ratio to the ambient fluid.

ρ Density of the fluid.

σ Electrical conductivity.

σ_0 Stefan-Boltzmann constant.

σ_s Scattering coefficient.

1 Introduction

Till date numerous authors discussed the flow of electrically conducting fluid in presence of transverse magnetic field and found interesting facts on the fluid flow and heat transfer. Magnetohydrodynamic (MHD) flow problems in fluid mechanics have been applied practically, for instance, in nuclear reactors Hartmann flow [1] reveal its application in the crossed-fields electromagnetic pumps. Consideration has been given to steady natural convection flow of electrically conducting fluid by various investigators such as Singh and Cowling [2], Dsa [3], Sears [4], Riley [5], Kuiken [6], Wilks [7], Hunt and Wilks [8] and Wilks and Hunt [9]. All these studies reported only heat transfer effects in the strong cross magnetic field. Very recently, Siddiqa *et al.* [10, 11] extended the above studies and consider mass transfer effects as well and discuss the numerical and analytical results for small Prandtl number $(<< 1)$.

The above cited investigations does not encounter thermal radiation effects which are important in context of space technology and processes involving high temperatures. The inclusion of thermal radiation effects in the energy equation leads to a highly nonlinear partial differential equation. In recent years, considering the Rosseland diffusion approximation, investigations on the natural convection flow as well as on the mixed convection flow of an optically dense gray viscous fluid past or along heated bodies of different geometries, such as, vertical and horizontal flat plate, cylinder, sphere, wavy surface

and axi-symmetic rotating and non-rotating bodies under different boundary conditions have been accomplished by Hossain *et al.* [12, 13], Hossain and Rees [14], Molla and Hossain [15] and Siddiqa *et al.* [16]. In these analysis consideration has been given to gray gases that emit and absorb but do not scatter thermal radiation. Its worth mentioning that in all the above studies the implicit finite difference method together with the Keller-box elimination technique posed by Keller [17] has been employed.

Liquid metals can be used in a range of applications because they are non-flammable, non-toxic and environmentally safe. This is why, liquid metals have number of technical applications in source exchangers, electronic pumps, ambient heat exchangers and also used as a heat engine fluid. Moreover, in nuclear power plants sodium, alloys, lead-bismuth and bismuth are extensively utilized heat transfer fluids (see [18]). Besides that, mercury play its role as a fluid in high-temperature Rankine cycles and also used in reactors in order to reduce the temperature of the system. For power plants which are exerted at extensively high temperature, sodium is treated as heat-engine fluid. Thus, due to the industrial and technical importance of liquid metals, Prandtl number Pr is taken to be 0.005 (sodium), 0.05 (lithium) and 0.01 (mercury) at typical operating temperatures (see Hunt and Wilks [8]).

In the strong cross magnetic field thermal radiation effects are not considered so far in the literature. Therefore, in the present analysis natural convection flow along a semi-infinite vertical plate of electrically conducting and optically dense gray fluid is studied in the presence of strong cross magnetic field and thermal radiation. Attention has been given to the special kind of fluids having low Prandtl number. The governing equations are reduced to convenient form by the introduction of SFF and PVF. Thus, the equations obtained by the former formulation (i.e. SFF) have been simulated by the implicit finite difference method along with the Keller-box scheme and the later one (i.e. PVF) is simulated by direct finite difference method together with Gaussian elimination technique. For the entire range of local Hartmann parameter, ξ, i.e. for $0 \leq \xi \leq \infty$, full numerical solutions are obtained with the two methods mentioned above. On the other hand, solutions for small and large ξ are also obtained with the help of series solution method and implicit finite difference (Keller-box) method, respectively. Consequently, the numerical results obtained for small, large and all ξ regions. The results are interpreted and compared graphically in view of wall shear stress and heat transfer rate by varying several physical parameters.

2 Mathematical Formulation

Consider steady state 2D natural convection flow of viscous fluid over a semi-infinite vertical surface of an electrically conducting and optically dense gray fluid in the presence of strong cross magnetic field having strength B_0. The surface temperature of the flat plate, T_w, is assumed to be higher than the ambient fluid temperature, T_∞. All the thermo-physical fluid properties are considered to be constant and viscous dissipation effects are neglected. Further, it is assumed that ratio of thermal diffusivity to magnetic diffusivity is small, in order to avoid perturbation in basic normal field. The coordinate system and flow configuration of the problem are shown in Fig. 1.

Using above assumptions and Boussinesq approximation, the boundary layer equations for conservation of mass, momentum and energy can be written as:

$$\frac{\partial u}{\partial x}+\frac{\partial v}{\partial y}=0 \tag{1}$$

$$u\frac{\partial u}{\partial x}+v\frac{\partial u}{\partial y}=\nu\frac{\partial^2 u}{\partial y^2}-\frac{\sigma B_0^2}{\rho}u+g\beta\left(T-T_\infty\right) \tag{2}$$

$$u\frac{\partial T}{\partial x}+v\frac{\partial T}{\partial y}=\alpha\left(\frac{\partial^2 T}{\partial y^2}-\frac{1}{\kappa}\frac{\partial q_r}{\partial y}\right) \tag{3}$$

where u and v are the x and y-components of the velocity field, respectively, in the momentum boundary layer, T the temperature of the fluid in the thermal boundary layer, ν the kinematic viscosity of the fluid, σ the electrical conductivity, B_0 the magnetic field normal to the plate, ρ the density of the fluid, g the acceleration due to gravity, κ the thermal conductivity, α the thermal diffusivity and β the coefficient of volumetric expansion. Here, it is assumed that the applied magnetic field is large enough that buoyancy force becomes more dominant as compared to inertial forces. The term q_r in energy equation represents radiative heat flux in the y-direction. The optically thick radiation limit (known as Rosseland diffusion

approximation (see Ozisik [19])) is considered here in order to reduce the complexity of the problem and to provide a means of comparison with further studies that might employ a more detailed representation for the radiative heat flux. Due to this assumption, the radiative heat flux q_r is as given in (4).

$$q_r = -\frac{4\sigma_0}{3(a+\sigma_s)}\frac{\partial T^4}{\partial y} \tag{4}$$

which is valid only for intensive absorption. In Eq. (4) a is the Rosseland mean absorption coefficient, σ_s the scattering coefficient and σ_0 the Stefan-Boltzmann constant.

The boundary conditions to be satisfied are

$$\begin{gathered} u(0,x) = v(0,x) = 0, \quad T(0,x) = T_w \\ u(\infty,x) \to 0, \quad T(\infty,x) \to T_\infty \end{gathered} \tag{5}$$

Now we will concentrate on the solution of the boundary layer problem posed in Eqs. (1)-(5). For this purpose stream function and primitive variable formulations are introduced which reduces the boundary layer Eqs. (1)-(5) to suitable form that can be used further to apply the appropriate numerical schemes.

3 Stream function formulation (SFF)

With the help of SFF we intend to transform the Eqs. (1)-(5) into a system of non-similar equations, which is appropriate for the entire region i.e. from the leading edge to the downstream region. Therefore, following continuous transformations are employed which were initiated by Hunt and Wilks [8] for the semi-infinite vertical flat plate:

$$\begin{gathered} \psi = \nu Gr_x^{1/4}(1+\xi)^{-1/4} f(\eta,\xi), \quad \theta(\eta,\xi) = \frac{T-T_\infty}{T_w-T_\infty}, \\ \eta = \frac{y}{x} Gr_x^{1/4}(1+\xi)^{-1/4}, \quad \xi = \frac{\left(\sigma B_0^2/\rho\right)^2}{g\beta(T_w-T_\infty)}x, \\ Gr_x = \frac{g\beta(T_w-T_\infty)x^3}{\nu^2} \end{gathered} \tag{6}$$

where ψ is the stream function which satisfies the equation of continuity (1) and is defined as

$$u = \frac{\partial \psi}{\partial y} \quad \text{and} \quad v = -\frac{\partial \psi}{\partial x} \tag{7}$$

In Eq. (6) η is a dimensionless pseudo-similarity variable, Gr_x the Grashof number which measures the ratio of buoyancy force to the viscous force acting on the optically dense gray fluid and ξ is termed as local Hartmann parameter which gives the ratio of magnetic force to the buoyancy force in the absence of thermal and viscous diffusivity. Thus introducing (6) into the governing Eqs. (1)-(5), we acquire the following non-similar equations:

$$\begin{aligned} &f''' + \frac{3+2\xi}{4(1+\xi)} f f'' - \frac{1}{2(1+\xi)} f'^2 + (1+\xi)\theta \\ &- \xi^{1/2}(1+\xi)^{1/2} f' = \xi \left(f' \frac{\partial f'}{\partial \xi} - f'' \frac{\partial f}{\partial \xi} \right) \end{aligned} \tag{8}$$

$$\begin{aligned} &\frac{1}{\mathrm{Pr}} \left\{ \left(1 + \frac{4}{3} R_d \left(1 + \triangle\theta\right)^3 \right) \theta' \right\}' + \frac{3+2\xi}{4(1+\xi)} f \theta' \\ &= \xi \left(f' \frac{\partial \theta}{\partial \xi} - \theta' \frac{\partial f}{\partial \xi} \right) \end{aligned} \tag{9}$$

where Pr is the Prandtl number which measures the ratio of momentum diffusivity and thermal diffusivity, R_d the Plank constant or the thermal radiation parameter which acts as a heat source due to the thermal radiation and θ_w the surface temperature parameter which gives the ratio of the surface temperature to the ambient fluid temperature. Mathematical expressions for these parameters are:

$$\mathrm{Pr} = \frac{\nu}{\alpha}, \quad R_d = \frac{4\sigma_0 T_\infty^3}{\kappa (a + \sigma_s)}, \quad \theta_w = \frac{T_w}{T_\infty}, \quad \triangle = \theta_w - 1 \tag{10}$$

The boundary conditions to be satisfied are

$$\begin{gathered} f(0,\xi) = f'(0,\xi) = 0, \quad \theta(0,\xi) = 1 \\ f'(\infty,\xi) \to 0, \quad \theta(\infty,\xi) \to 0 \end{gathered} \tag{11}$$

It needs to mention here that Hunt and Wilks [8] discuss the above posed problem (8)-(11) in the absence of thermal radiation. In their investigation, the authors obtain the full numerical solutions via algorithm based upon Keller box technique [17]. They firmly emphasized on the fact that for sufficiently large local Hartmann parameter, ξ, matched asymptotic expansion technique is appropriate in order to achieve consistency. However, for small ξ ordinary perturbation technique is employed. For $R_d = 0.0$ present model reduces to the one investigated by Hunt and Wilks [8].

At this position shear stress and heat transfer rate can be calculated which are important physical quantities from engineering point of view. The mathematical relations for these quantities are:

$$\tau_w = \xi^{1/4}(1+\xi)^{-3/4} f''(0,\xi) \tag{12}$$

$$Q = -\left(1 + \frac{4}{3} R_d \theta_w^3\right) \xi^{-1/4}(1+\xi)^{-1/4} \theta'(0,\xi) \tag{13}$$

The formulation obtained in (8)-(11) have been integrated numerically via implicit finite difference method along with the Keller-box scheme, introduced by Keller and Cebeci [20] and subsequently their idea was exposed well by Cebeci and Bradshaw [21]. A brief discussion on the development of the algorithm of implicit finite difference method together with Keller-box scheme is as under.

To apply the aforementioned method, the non-similar Eqs. (8)-(9) subject to the boundary conditions

(11) are initially reduce to the system of first order equations in η as described below:

$$\begin{gathered} f' = g \\ g' = w \\ w' + P_1(\xi) f w - P_2(\xi) g^2 + P_3(\xi)\theta - P_4(\xi) g = \xi \left(g \frac{\partial g}{\partial \xi} - w \frac{\partial f}{\partial \xi} \right) \\ \theta' = p \\ \frac{1}{\mathrm{Pr}} \left\{ \left(1 + \frac{4}{3} R_d (1 + \triangle\theta)^3 \right) p \right\}' + P_1(\xi) f p = \xi \left(g \frac{\partial \theta}{\partial \xi} - p \frac{\partial f}{\partial \xi} \right) \end{gathered} \tag{14}$$

where

$$\begin{gathered} P_1(\xi) = \frac{3 + 2\xi}{4(1+\xi)}, \quad P_2(\xi) = \frac{1}{2(1+\xi)}, \\ P_3(\xi) = 1 + \xi, \quad P_4 = \xi^{1/2}(1+\xi)^{1/2} \end{gathered}$$

The boundary conditions are

$$f_0^j = 0, \quad g_0^j = 0, \quad \theta_0^j = 1, \quad g_M^j = 0, \quad \theta_M^j = 0 \tag{15}$$

The primes in (14) denote the derivatives with respect to η and mesh points in the η and ξ direction are symbolized by η_i for $i = 1, 2, 3, \cdots, M$ and ξ_j for $j = 1, 2, 3, \cdots, N$, respectively. Afterwards, standard finite difference formulas are utilized to approximate the functions. Central difference approximations are made such that the equations involving ξ explicitly are centered at $\left(\xi_{j-1/2}, \eta_{i-1/2}\right)$ and the remainder at $\left(\xi_j, \eta_{i-1/2}\right)$, with $\eta_{i-1/2} = (\eta_i + \eta_{i-1})/2$. Ultimately, a set of nonlinear differential equations are obtained for the unknowns at ξ_j in terms of their previous station at ξ_{j-1}. The resulting finite difference equations are non-linear algebraic equations and are linearized by adopting Newton-Raphson method and finally solutions are acquired by using block-elimination algorithm. Numerical procedure is initiated at $\xi = 0.0$, when distribution curves are provided for those unknown variables which emerges at the time of reduction of order. Keller box scheme takes the charge to solve the ordinary differential equa-

tions. Having obtained the leading edge solution it is possible to march step by step along the boundary layer. Numerical computations are done repeatedly until some convergence criteria is achieved. For the present problem, convergence criteria is taken to be 10^{-6}, i.e. when $\mid \delta f^k \mid \leq 10^{-6}$ where k denotes the iteration number. Due to numerical complexities, non-uniform grid is chosen in the η-direction instead of uniform grid, which is defined by $\eta_i = \sinh(i/a)$ with $a = 100$ and $N = 301$, whereas in the ξ direction grid size, $\triangle\xi$, is taken to be 0.02. This method has successfully been employed by Hossain *et al.* [12, 13].

In the following section, we shall discuss and apply PVF on the governing Eqs. (1)-(5). This formulation is also used to obtain solution for entire ξ regime.

4 Primitive variable formulation (PVF)

Consider the following primitive variable formulations which are used to transform the Eqs. (1)-(5) into suitable form over which direct finite difference method along with the Gaussian elimination technique can be applied.

$$\begin{aligned} u &= \frac{\nu Gr_x^{1/2}(1+\xi)^{-1/2}}{x}\bar{u}, \quad v = \frac{\nu Gr_x^{1/4}(1+\xi)^{-1/4}}{x}\bar{v}, \\ \bar{y} &= \frac{Gr_x^{1/4}(1+\xi)^{-1/4}}{x}y, \quad \theta = \frac{T-T_\infty}{T_w-T_\infty}, \\ \xi &= \frac{\left(\sigma B_0^2/\rho\right)^2}{g\beta\left(T_w-T_\infty\right)}x, \quad Gr_x = \frac{g\beta\left(T_w-T_\infty\right)x^3}{\nu^2} \end{aligned} \tag{16}$$

Using (16) in (1)-(5) one obtains

$$\frac{\bar{u}}{2(1+\xi)} + \xi\frac{\partial\bar{u}}{\partial\xi} - \frac{\bar{y}}{4}\left(\frac{1+2\xi}{1+\xi}\right)\frac{\partial\bar{u}}{\partial\bar{y}} + \frac{\partial\bar{v}}{\partial\bar{y}} = 0 \tag{17}$$

$$\frac{\bar{u}^2}{2(1+\xi)}+\xi\bar{u}\frac{\partial\bar{u}}{\partial\xi}+\left[\bar{v}-\frac{\bar{y}\bar{u}}{4}\left(\frac{1+2\xi}{1+\xi}\right)\right]\frac{\partial\bar{u}}{\partial\bar{y}} = \frac{\partial^2\bar{u}}{\partial\bar{y}^2}-\xi^{1/2}(1+\xi)^{1/2}\bar{u}+(1+\xi)\theta \tag{18}$$

$$\xi\bar{u}\frac{\partial\theta}{\partial\xi}+\left[\bar{v}-\frac{\bar{y}\bar{u}}{4}\left(\frac{1+2\xi}{1+\xi}\right)\right]\frac{\partial\theta}{\partial\bar{y}} = \frac{1}{\Pr}\frac{\partial}{\partial\bar{y}}\left[\left(1+\frac{4}{3}R_d(1+\triangle\theta)^3\right)\frac{\partial\theta}{\partial\bar{y}}\right] \tag{19}$$

The corresponding boundary conditions are

$$\bar{u}(0,\xi)=\bar{v}(0,\xi)=0,\quad \theta(0,\xi)=1$$
$$\bar{u}(\infty,\xi)\to 0,\quad \theta(\infty,\xi)\to 0 \tag{20}$$

Practically, the physical quantities of interest are shearing stress and rate of heat transfer, which can be obtained from the following relations, respectively.

$$\tau_w=\xi^{1/4}(1+\xi)^{-3/4}\left(\frac{\partial\bar{u}}{\partial\bar{y}}\right)_{\bar{y}=0} \tag{21}$$

$$Q=-\left(1+\frac{4}{3}R_d\theta_w^3\right)\xi^{-1/4}(1+\xi)^{-1/4}\left(\frac{\partial\theta}{\partial\bar{y}}\right)_{\bar{y}=0} \tag{22}$$

The parabolic partial differential equations obtained in (17)-(20) have been integrated numerically with the aid of direct finite difference method along with the Gaussian elimination technique.

Now a brief discussion is carried out on the establishment of the algorithm of direct finite difference method. The partial differential equations (17)-(20) are discretized for numerical scheme using central-difference for diffusion terms and backward difference for the convection terms. Finally a system of

algebraic equations is obtained as given below:

$$\begin{aligned}
&\frac{\bar{u}_{i,k}^{2}}{2(1+\xi_k)}+\xi_k\bar{u}_{i,k}\frac{\bar{u}_{i,k}-\bar{u}_{i,k-1}}{\triangle\xi}+\left[\bar{v}_{i,k}-\frac{\bar{y}_i\bar{u}_{i,k}}{4}\left(\frac{1+2\xi_k}{1+\xi_k}\right)\right]\\
&\frac{\bar{u}_{i+1,k}-\bar{u}_{i-1,k}}{2\triangle\bar{y}}=\frac{\bar{u}_{i+1,k}-2\bar{u}_{i,k}+\bar{u}_{i-1,k}}{(\triangle\bar{y})^2}\\
&-\xi_k^{1/2}(1+\xi_k)^{1/2}\bar{u}_{i,k}+(1+\xi_k)\theta_{i,k}
\end{aligned}\tag{23}$$

$$\begin{aligned}
\xi_k\bar{u}_{i,k}\frac{\theta_{i,k}-\theta_{i,k-1}}{\triangle\xi}+\left[\bar{v}_{i,k}-\frac{\bar{y}_i\bar{u}_{i,k}}{4}\left(\frac{1+2\xi_k}{1+\xi_k}\right)\right]\frac{\theta_{i+1,k}-\theta_{i-1,k}}{2\triangle\bar{y}}\\
=\frac{1}{\mathrm{Pr}}\left(1+\frac{4}{3}R_d(1+\triangle\theta_{i,k})^3\right)\frac{\theta_{i+1,k}-2\theta_{i,k}+\theta_{i-1,k}}{(\triangle\bar{y})^2}\\
+\frac{1}{\mathrm{Pr}}\left(4\triangle R_d(1+\triangle\theta_{i,k})^2\right)\left(\frac{\theta_{i+1,k}-\theta_{i-1,k}}{2\triangle\bar{y}}\right)^2
\end{aligned}\tag{24}$$

for $2\leq i\leq L-1$ and $1\leq k\leq L$. Subscripts i and k represent the grid points along the $\bar{y}$ and ξ directions respectively, whereas $\triangle\xi=\xi_k-\xi_{k-1}$ and $\triangle\bar{y}=\bar{y}_i-\bar{y}_{i-1}$ are the step sizes in their respective directions. The boundary conditions takes the form

$$\begin{aligned}
\bar{u}_{1,k}=\bar{v}_{1,k}=0,\quad \theta_{1,k}=1\\
\bar{u}_{L,k}=0,\quad \theta_{L,k}=0
\end{aligned}\tag{25}$$

Eqs. (23)-(25) leads to a tri-diagonal system of algebraic equations, which can be solved using Gaussian elimination method for the unknowns $\bar{u}$ and θ independently. In the computation, continuity equation is used to solve directly the normal velocity vector $\bar{v}$ by using the following discretization

$$\begin{aligned}
\bar{v}_{i,k}=\bar{v}_{i-1,k}+\frac{\bar{y}_i}{4}\left(\frac{1+2\xi_k}{1+\xi_k}\right)\left(\bar{u}_{i,k}-\bar{u}_{i-1,k}\right)\\
-\frac{\triangle\bar{y}}{4(1+\xi_k)}\left(\bar{u}_{i,k}+\bar{u}_{i-1,k}\right)-\frac{\xi_k\triangle\bar{y}}{\triangle\xi}\left(\bar{u}_{i,k}-\bar{u}_{i,k-1}\right)
\end{aligned}\tag{26}$$

The computation is started at $\xi = 0.0$ and then marches downstream implicitly. Here, 0.03 and 0.01 are choose for the ξ and $\bar{y}$ girds respectively. For a given value of ξ, the iterative procedure is stopped when the difference of present and the next computed value of unknown variable (such as velocity or temperature) is less than 10^{-6}. Very recently, this method has been used successfully by Siddiqa *et al.* [22] in order to investigate extensively high Prandtl number effects on the natural convection flow over an inclined flat plate with internal heat generation and variable viscosity. Molla *et al.* [23] also used this numerical scheme, efficiently, to study natural convection boundary layer flow over a vertical wavy frustum of a cone in the presence of thermal radiation.

Thus, in Fig. 2 the numerical results obtained by this method are compared with that obtained from stream function formulation. In this figure skin-friction, τ_w, and rate of heat transfer, Q, are drawn against ξ while other parameters are $R_d = 0.0, 1.0$ and 2.0, $\theta_w = 1.1$ and Pr=0.05. This figure ensures that excellent compatibility lies between PVF and SFF for the present circumstances.

Further consideration has been given to the regions, where the local Hartman parameter, ξ, is regarded to be small and large enough.

5 Asymptotic solutions for small and large ξ

In this section solution methodologies are discussed for small and large values of the local Hartmann parameter, ξ, and the results of both regions (small and large) are compared with solutions obtained in section (3).

5.1 Solutions for small ξ

Its worth mentioning that the boundary layer structure is expected to be similar near the leading edge of the plate. For small ξ, the magnetic force is weaker in magnitude as compared to the buoyancy forces. Therefore, in the vicinity of the plate the electrically conducting fluid feels the influence of buoyancy force more dominantly as compared to any other force. The limiting case $\xi \to 0$ in Eqs. (8)-(11) leads to the non-similar equations valid for small ξ therefore with this condition we get the following equations for small ξ:

$$f''' + \frac{3}{4} f f'' - \frac{1}{2} f'^2 + \theta - \xi^{1/2} f' = \xi \left(f' \frac{\partial f'}{\partial \xi} - f'' \frac{\partial f}{\partial \xi} \right) \tag{27}$$

$$\begin{aligned}&\frac{1}{\mathrm{Pr}}\left\{\left(1+\frac{4}{3}R_d\left(1+\triangle\theta\right)^3\right)\theta'\right\}'+\frac{3}{4}f\theta'\\&=\xi\left(f'\frac{\partial\theta}{\partial\xi}-\theta'\frac{\partial f}{\partial\xi}\right)\end{aligned}\tag{28}$$

The boundary conditions are

$$\begin{aligned}f(0,\xi)=f'(0,\xi)=0,\quad \theta(0,\xi)=1\\f'(\infty,\xi)\to 0,\quad \theta(\infty,\xi)\to 0\end{aligned}\tag{29}$$

In order to obtain the solution of the Eqs. (27)-(29), series solution method is adopted which is valid for sufficiently small local Hartmann parameter, ξ. Thus the unknown functions $f(\eta,\xi)$ and $\theta(\eta,\xi)$ are expressed as:

$$\begin{aligned}f(\eta,\xi)=f_0(\eta)+\xi^{1/2}f_1(\eta)+\cdots\\\theta(\eta,\xi)=\theta_0(\eta)+\xi^{1/2}\theta_1(\eta)+\cdots\end{aligned}\tag{30}$$

Substituting the above expansions into Eqs. (27)-(29) and equating the coefficients of like power of ξ, we get coupled equations for each order of ξ. For the present analysis, series solution is acquired up to $O(\xi^{1/2})$, in order to estimate the particular range of validity of series solution in contrast with the exact values. Leading order problem is given by the equations

$$f_0'''+\frac{3}{4}f_0f_0''-\frac{1}{2}f_0'^2+\theta_0=0\tag{31}$$

$$\frac{1}{\mathrm{Pr}}\left\{\left(1+\frac{4}{3}R_d\left(1+\triangle\theta_0\right)^3\right)\theta_0'\right\}'+\frac{3}{4}f_0\theta_0'=0\tag{32}$$

$$\begin{aligned} f_0(0) = f_0'(0) = 0, \quad \theta_0(0) = 1 \\ f_0'(\infty) \to 0, \quad \theta_0(\infty) \to 0 \end{aligned} \tag{33}$$

Similarly, for $O\left(\xi^{1/2}\right)$, $f_1(\eta)$ and $\theta_1(\eta)$ satisfies the following linear system subject to the homogeneous boundary conditions and is given by

$$f_1''' + \frac{3}{4} f_0 f_1'' - \frac{3}{2} f_0' f_1' + \frac{5}{4} f_0'' f_1 - f_0 + \theta_1 = 0 \tag{34}$$

$$\begin{aligned} &\frac{1}{\mathrm{Pr}} \left\{ \left(1 + \frac{4}{3} R_d \left(1 + \triangle \theta_0\right)^3 \right) \theta_1'' + 8 \triangle R_d \left(1 + \triangle \theta_0\right)^2 \theta_0' \theta_1' \right\} \\ &\quad + \frac{1}{\mathrm{Pr}} 4 \triangle R_d \left(1 + \triangle \theta_0\right) \left\{ \left(1 + \triangle \theta_0\right) \theta_0'' + 2 \triangle \theta_0'^2 \right\} \theta_1 \qquad (35) \\ &\quad + \frac{3}{4} f_0 \theta_1' - \frac{1}{2} f_0' \theta_1 + \frac{5}{4} f_1 \theta_0' = 0 \qquad (36) \end{aligned}$$

$$\begin{aligned} f_1(0) = f_1'(0) = 0, \quad \theta_1(0) = 0 \\ f_1'(\infty) \to 0, \quad \theta_1(\infty) \to 0 \end{aligned} \tag{37}$$

It can be seen that system of equations given in (31)-(33) and (34)-(37) are coupled and can be integrated sequentially with the help of Runge Kutta initial value solver introduced by Butcher [24] in connection with the iterative scheme of Nachtsheim and Swiegert [25]. In the light of physical parameters occurred in the present problem, pair of equations (31)-(33) and (34)-(37) are solved numerically and graphed in terms of shear stress and rate of heat transfer. These physical quantities can be computed from the following relations

$$\tau_w = \xi^{1/4} \left(f_0''(0) + \xi^{1/2} f_1''(0) + \cdots \right) \tag{38}$$

$$Q = -\left(1+\frac{4}{3}R_d\theta_w^3\right)\xi^{-1/4}\left(\theta_0'(0)+\xi^{1/2}\theta_1'(0)+\cdots\right) \tag{39}$$

Now, we readily draw our attention on the system of equations valid in the downstream region, where local Hartmann parameter ξ is treated to be sufficiently large.

5.2 Solution for large ξ

For the downstream region (large ξ), the boundary layer is developed primarily due to the magnetic forces parallel to the surface of the plate. It should be noted that far from the surface of the flat plate buoyancy force effects are less effective whereas magnetic force looks to be more authoritative there. In this section, attention shall be given to the behavior of the solution to equations (8)-(11) when ξ is large. For this, the dominant terms are balanced in magnitude and appropriate governing equations, as $\xi \to \infty$, are found to be

$$\frac{1}{\xi}f''' + \frac{1}{2\xi}ff'' + \theta - f' = \left(f'\frac{\partial f'}{\partial \xi} - f''\frac{\partial f}{\partial \xi}\right) \tag{40}$$

$$\frac{1}{\Pr}\left\{\left(1+\frac{4}{3}R_d\left(1+\triangle\theta\right)^3\right)\theta'\right\}' + \frac{1}{2}f\theta' = \xi\left(f'\frac{\partial \theta}{\partial \xi} - \theta'\frac{\partial f}{\partial \xi}\right) \tag{41}$$

The boundary conditions to be satisfied are

$$\begin{gathered} f(0,\xi) = f'(0,\xi) = 0, \quad \theta(0,\xi) = 1 \\ f'(\infty,\xi) \to 0, \quad \theta(\infty,\xi) \to 0 \end{gathered} \tag{42}$$

Here, Eqs. (40)-(42) are solved numerically by employing implicit finite difference method along with the Keller box technique [17]. Complete details of the method of solution are illustrated well in the preceding section. However, few facts needs to highlight here. In numerical computation, condition at infinity is archived by selecting a suitable value of η. In the present analysis, η is chosen to be 5.0 or less,

in order to achieve the asymptotic numeric values. Reasonable choice of net spacing $\triangle\eta(=\eta_i-\eta_{i-1})$ and $\triangle\xi(=\xi_j-\xi_{j-1})$ makes the numerical results convergent and comparable which can be seen clearly in the Figs. (3)-(5).

The fundamental features of the flow, the shear stress and the heat transfer rate, are discussed for this region with the help of following expressions:

$$\tau_w = \xi^{-1/2} f''(0,\xi) \tag{43}$$

and

$$Q = -\left(1+\frac{4}{3}R_d\theta_w^3\right)\xi^{-1/2}\theta'(0,\xi) \tag{44}$$

Now, discussion is carried out on the numerical results obtained in terms of wall shear stress, rate of heat transfer, velocity and temperature distributions in effect of the physical parameters such as radiation parameter, R_d, surface temperature parameter, θ_w and Prandtl number, Pr. Graphically, an excellent agreement is found when solutions are compared for small, large and all ξ regions. It should be noted that all the results are obtained for liquid metals for which Prandtl number is considered to be small.

6 Results and discussion

Underlying problem deals with the free convection flow of electrically conducting and optically dense gray fluid over a vertical plate in a strong cross-field. Here we use the stream function formulation as well as the primitive variable formulation to convert the boundary layer equations in to a suitable form. Thus, the equations obtained by the former formulation have been simulated by the implicit finite difference method along with the Keller-box scheme; and the later one is simulated by direct finite difference method together with Gaussian elimination technique. Full numerical solutions for the whole range of local Hartmann parameter, ξ, are obtained from both the methods mentioned above. However, for the case of upstream (small ξ) and downstream (large ξ) regions numerical solutions are obtained respectively, with the help of series solution method and implicit finite difference (Keller-box) method.

Table 1. Numerical values of coefficients of skin-friction with $R_d = 0.0$ and $\theta_w = 1.1$

	$f_0''(0)$		$f_1''(0)$	
Pr	Hunt and Wilks [8]	Present	Hunt and Wilks [8]	Present
1.0	0.64219	0.64205	-0.21005	-0.20991
0.72	0.79670	0.79633	-0.27034	-0.27017
0.5	1.00855	1.00828	-0.35656	-0.35644
0.25	1.56129	1.56106	-0.59359	-0.59345
0.1	2.71693	2.71670	-1.11640	-1.11623
0.05	4.06165	4.06133	-1.74438	-1.74404
0.025	5.99574	5.99504	-2.66289	-2.66191
0.01	9.87754	9.87488	-4.52789	-4.52348
0.005	14.27932	14.26614	-6.65618	-6.63935

Details of the numerical computation is discussed in the earlier section. Physical interpretation has been given for the parameters controlling the flow within the boundary layer. It needs to mention that liquid metals are used as a working fluid which have tempting applications because of their ability to reduce temperature of the system. Due to the industrial and technical importance of such fluids, here Prandtl number Pr is taken to be 0.005, 0.05 and 0.01 which are appropriate for liquid metals, namely, sodium, lithium and mercury respectively.

As mentioned earlier, Hunt and Wilks [8] studied the same problem but in the absence of thermal radiation ($R_d = 0.0$) and the present numerical results are compared with them. Numerical values of the coefficients of skin friction $f_0''(0)$ and $f_1''(0)$ and heat transfer $\theta_0'(0)$ and $\theta_1'(0)$ thus obtained for $R_d = 0.0$, $\theta_w = 1.1$ are entered in Table 1 and compared with that of Hunt and Wilks [8], for several values of Pr. Comparison shows excellent agreement between the present work and results given by Hunt and Wilks [8].

6.1 Effect of physical parameters Pr, R_d and θ_w on skin-friction and rate of heat transfer:

The influence of fluids having Prandtl number Pr = 0.005, 0.05 and 0.01, on shear stress, τ_w, and heat transfer rate, Q, is shown pictorially in Fig. 3 against ξ. However, other physical parameters are taken

Table 2. Numerical values of coefficients of heat transfer with $R_d = 0.0$ and $\theta_w = 1.1$

	$\theta_0'(0)$		$\theta_1'(0)$	
Pr	Hunt and Wilks [8]	Present	Hunt and Wilks [8]	Present
1.0	-0.56715	-0.56712	0.13670	0.13645
0.72	-0.59472	-0.59472	0.14593	0.14536
0.5	-0.62390	-0.62389	0.15599	0.15551
0.25	-0.67404	-0.67400	0.17377	0.17328
0.1	-0.72780	-0.72774	0.19325	0.19272
0.05	-0.75902	-0.75895	0.20462	0.20407
0.025	-0.78307	-0.78300	0.21338	0.21282
0.01	-0.80593	-0.80590	0.22167	0.22144
0.005	-0.81805	-0.81982	0.22606	0.21764

to be $R_d = 1.0$ and $\theta_w = 1.1$. From Fig. 3(a) it is observed that increase in Prandtl number, Pr, leads to the reduction in the magnitude of the shear-stress and on the contrary Fig. 3(b) depicts that rate of heat transfer enhances. It is expected, because of an increase in the value of Pr thermal conductivity of the fluid diminishes, which conclusively lessens the magnitude of frictional forces between the viscous layers. Due to this, shear-stress gradually becomes less strong while rate of heat transfer get enough support to grow firmly, in the vicinity of the plate. It is also clear from the figures that momentum and thermal boundary layer thicknesses increases considerably due to the increment in Pr.

Now, the effect of thermal radiation parameter (Plank constant), $R_d = 0.0, 1.0$ and 4.0 is illustrated in Fig. 4 for $\theta_w = 2.0$ and Pr = 0.05 on skin-friction, τ_w, and heat transfer rate, Q. In the absence of thermal radiation effects i.e. for $R_d = 0.0$, the present results reduces to the one obtained by Hunt and Wilks [8]. Both Figs. 4(a) and 4(b) depicts that shear-stress and rate of heat transfer enhances considerably owing to increase in the thermal radiation parameter, R_d. Due to the intense thermal radiation inside the boundary layer, rate of energy transport of the fluid is increased sharply which in turn give rise to the temperature of the fluid in the surrounding of the plate surface. This is why, heat transfer and shear stress get stronger, inside the boundary layer. Moreover, momentum boundary layer thickness happens to reduces as we increase thermal radiation parameter, R_d.

The variation of shear stress, τ_w, and rate of heat transfer, Q, is inspected for $\theta_w = 1.1, 2.0$ and 3.0 in Fig. 5 with $R_d = 2.0$ and Pr = 0.05. Here, notable enhancement is recorded for both shear stress and heat transfer rate as we intensify the surface temperature parameter θ_w. Such a behavior is possible because increment in surface temperature parameter, θ_w, leads to an increase in the motion of the fluid particles. This rapid increase in the motion of the fluid accelerates the flow rate near the plate. Thus, surface temperature parameter is responsible for the upraise in the temperature of the fluid and ultimately wall shear stress and heat transfer rate increases. Further, impact of surface temperature parameter tends to decrease the momentum boundary layer thickness.

6.2 Effect of R_d, θ_w and ξ on velocity and temperature distributions:

Here, we focus our attention on the effects of various physical parameters that appear in the problem and interpret them in terms of velocity and temperature profiles for the case of liquid metals.

Graphical representation of numerical values of velocity and temperature profiles are shown in Fig. 6, for thermal radiation parameter $R_d = 0.0, 1.0$ and 2.0 and $\theta_w = 1.1, 1.7$ while other parameters take the values Pr = 0.05 and $\xi = 1.0$. Here, solid lines display the results for $\theta_w = 1.1$ whereas broken curves present the results obtained for $\theta_w = 1.7$. It is inferred from the figure that thermal radiation and surface temperature parameters have notable effects on the velocity and temperature profiles as electrically conducting and optically dense gray fluid is accelerated rapidly near the surface of the plate due to the enhancement in the values of R_d and θ_w. Likewise, we find that the thickness of the momentum and thermal boundary layer becomes thinner as surface temperature, θ_w, increases. This result is anticipated since radiation and surface temperature enhancement extensively adds up thermal energy to the fluid, which leads to an increase in the temperature of the fluid and eventually causes the velocity and temperature profiles to increases inside the boundary layer.

Finally, we draw our attention towards the influence of local Hartmann parameter ξ. In Fig. 7, velocity and temperature distributions are depicted for $\xi = 0.0, 1.0$ and 10.0 while remaining parameters are $R_d = 1.0$, $\theta_w = 1.1$ and Pr=0.05. It is observed that velocity of the fluid decreases exclusively for the increase in the local Hartmann parameter ξ whereas temperature of the fluid tends to increase. Near the vicinity of the plate it is observed that velocity shoots up sharply and after attaining its maxima it settles down to its asymptotic values. The maxima occurs at 1.09008, 0.950407 and 0.946084 for $\xi = 0.0, 1.0$

and 10.0 respectively, which shows that velocity reduces effectively and numerical experiments shows that for $\xi = 10.0$, we achieve asymptotic velocity profile. In addition, it is noticed that in Fig. 7(a) velocity curve for $\xi = 0.0$ intersect the other curves at $\eta = 0.646605$ and decreases more quickly as compared to others. Conclusively, we can say that momentum boundary layer thickness increase for the increase in the values of ξ. Physically it happens since increment in the local Hartmann parameter, ξ, causes the magnitude of buoyancy forces to become less effective as compared to the magnetic forces that play dominant role when ξ is large and as a result velocity decreases significantly. Moreover, velocity distribution diminishes by 13.2386% as ξ increases from 0.0 to 10.0.

7 Conclusions

In this paper, we have studied the thermal radiation interaction on the two-dimensional free convection flow of an electrically conducting and optically dense gray viscous incompressible fluid over a semi-infinite vertical flat surface. The problem is studied under the influence of strong cross-field and consideration has been given to those working fluids which act as liquid metals. For entire range of local Hartmann number, ξ, the governing equations are reduced to parabolic partial differential equations using SFF and PVF which are then integrated employing the Keller box method and the direct finite difference method. Asymptotic solutions are also obtained for smaller and larger values of ξ. The numerical values thus obtained are discussed in terms of various physical parameters, such as, thermal radiation parameter, R_d, surface temperature parameter, θ_w, local Hartmann parameter, ξ, and Prandtl number, Pr. Velocity and temperature distributions are also analyzed critically in effect of several parameters. It is found that wall shear stress and heat transfer rate enhances owing to the increase in the radiation parameter, R_d, and surface temperature parameter θ_w. However, velocity and temperature profiles drawn for local Hartmann parameter, ξ, show that asymptotic profile is achieved at $\xi = 10.0$.

References

[1] Hartmann, J., 1937. “Hg-dynamics I: Theory of the laminar flow of an electrically conductive liquid in a homogeneous magnetic field”, *K. Dan. Vidensk. Selsk. Mat. Fys. Medd.*, 15, pp. 1-28.

[2] Singh, R. K., and Cowling, T. G., 1963. “Thermal convection in magnetohydrodynamics”, *Q. J. Mech. Appl. Math.*, 16, pp. 1-15.

[3] Dsa, E. R., 1967. "Magnetohydrodynamic free convection in a strong cross-field", *Z. Angew. Math. Phys.*, 18, pp. 106-115.

[4] Sears, W. R., 1966. "The boundary layer in crossed-fields MHD", *J. Fluid Mech.*, 25, pp. 229-240.

[5] Riley, N., 1964. "Magnetohydrodynamic free convection", *J. Fluid Mech.*, 18, pp. 577-586.

[6] Kuiken, H. K., 1970. "Magnetohydrodynamic free convection in a strong cross field", *J. Fluid Mech.*, 40, pp. 21-38.

[7] Wilks, G., 1976. "Mangnetohydrodynamic free convection about a semi-infinite vertical plate in a strong cross field", *ZAMP*, 27, pp. 621-631.

[8] Hunt, R., and Wilks, G., 1981. "Low Prandtl number magnetohydrodynamic natural convection in a strong cross field", *Numerical Heat Transfer*, 4, pp. 303-316.

[9] Wilks, G., and Hunt, R., 1984. "Magnetohydrodynamic free convection flow about a semi-infinite plate at whose surface the heat flux is uniform", *ZAMP*, 35, pp. 34-49.

[10] Siddiqa, S., Hossain, M. A., and Pop, I., 2012. "Conjugate thermal and mass diffusion effect on natural convection flow in presence of strong cross magnetic field", *Int. J. Heat Mass Transfer*, 55, pp. 5120-5132.

[11] Siddiqa, S., Hossain, M. A., Saha, S. C., 2012. "Double diffusive magneto-convection fluid flow in a strong cross magnetic field with uniform surface heat and mass flux", *J. Heat Transfer*, 134, pp. 1145061-1145069.

[12] Hossain, M. A., Kutubuddin, M., and Pop, I., 1999. "Effect of conduction-radiation interaction on the mixed convection flow from a horizaontal cylinder", *Heat Mass Transfer*, 35, pp. 307-314.

[13] Hossain, M. A., Anghel, M., and Pop, I., 2002. "Thermal radiation effect on free convection over axissymmetric body with application to a rotating hemisphere", *Arch. Mech.*, 54, pp. 55-74.

[14] Hossain, M. A., and Rees, D. A. S., 1998. "Radiation conduction interaction on mixed convection flow along a slender vertical cylinder", *AIAA J. Thermophys. Heat Transfer*, 12, pp. 611-614.

[15] Molla, M. M., and Hossain, M. A., 2007. "Radiation effect on mixed convection laminar flow along a vertical wavy surface", *Int. J. Therm. Sci.*, 46, pp. 926-935.

[16] Siddiqa, S., Asghar, S., and Hossain, M. A., 2011. "Radiation effects on natural convection flow over an inclined flat plate with temperature-dependent viscosity", *J Mech. Engg. Sci.*, 225, pp. 407-419.

[17] Keller, H. B., 1978. "Numerical methods in boundary layer theory", *Annu. Rev. Fluid Mech.*, 10, pp. 417-433.

[18] Hammitt, F. G., 1960. "Liquid metal cavitation-problems and desired research", The univeristy of Michigan.

[19] Ozisik, M. N., 1973. "Thermal radiation transfer and interactions with conduction and convection", John Wiley & Sons, New York.

[20] Keller, H. B., and Cebeci, T., 1971. "Accurate numerical methods for boundary layer flows, I. Two-dimensional laminar flows, Lecture notes in physics", Proceedings of second international conference on numerical methods in fluid dynamics, Springer-Verlag.

[21] Cebeci, T., and Bradshaw, P., 1984. "Physical and computational aspects of convective heat transfer", Springer, New York.

[22] Siddiqa, S., Asghar, S., and Hossain, M. A., 2010. "Natural convection flow over an inclined flat plate with internal heat generation and variable viscosity", *Math. and Comp. Model.*, 52, pp. 1739-1751.

[23] Molla, M. M., Hossain, M. A., and Gorla, R. S. R., 2009. "Radiation effect on natural convection boundary layer flow over a vertical wavy frustum of a cone", *Part C: J. Mech. Eng. Sci.*, 223, pp. 1605-1614.

[24] Butcher, J. C., 1964. "Implicit Runge-Kutta process", *Math. Comput.*, 18, pp. 50-55.

[25] Nachtsheim, P. R., Swiegert, P., 1965. "Satisfaction of asymptotic boundary conditions in numerical solutions of system of nonlinear equations of the boundary layer type", *NASA TND-3004*.

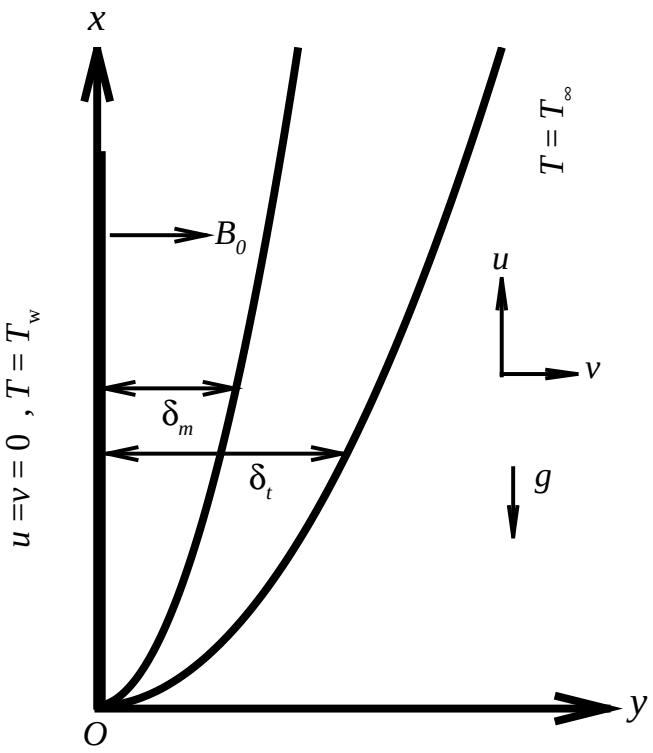

Fig. 1. Coordinate system and physical model

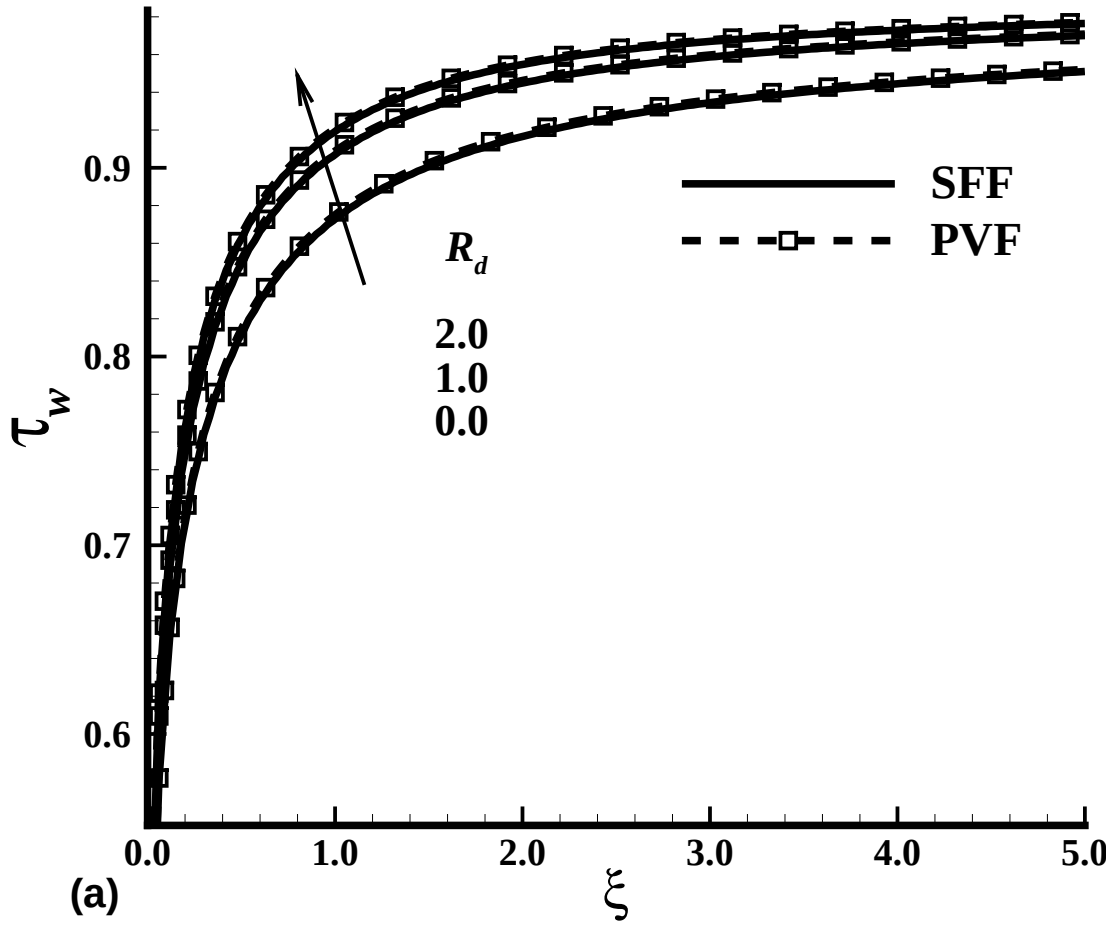

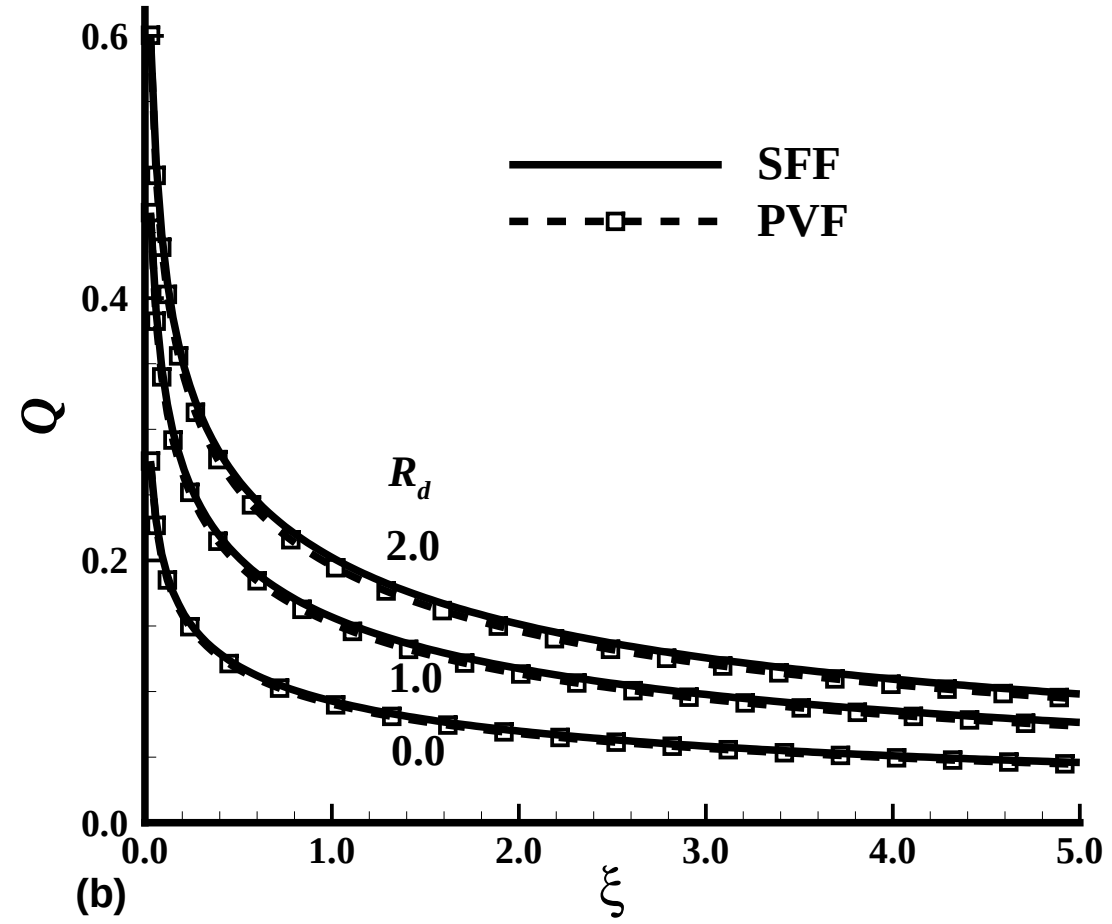

Fig. 2. (a) Variation of shear stress and (b) rate of heat transfer with ξ for $R_d = 0.0, 1.0, 2.0$ while Pr = 0.05 and $\theta_w = 1.1$

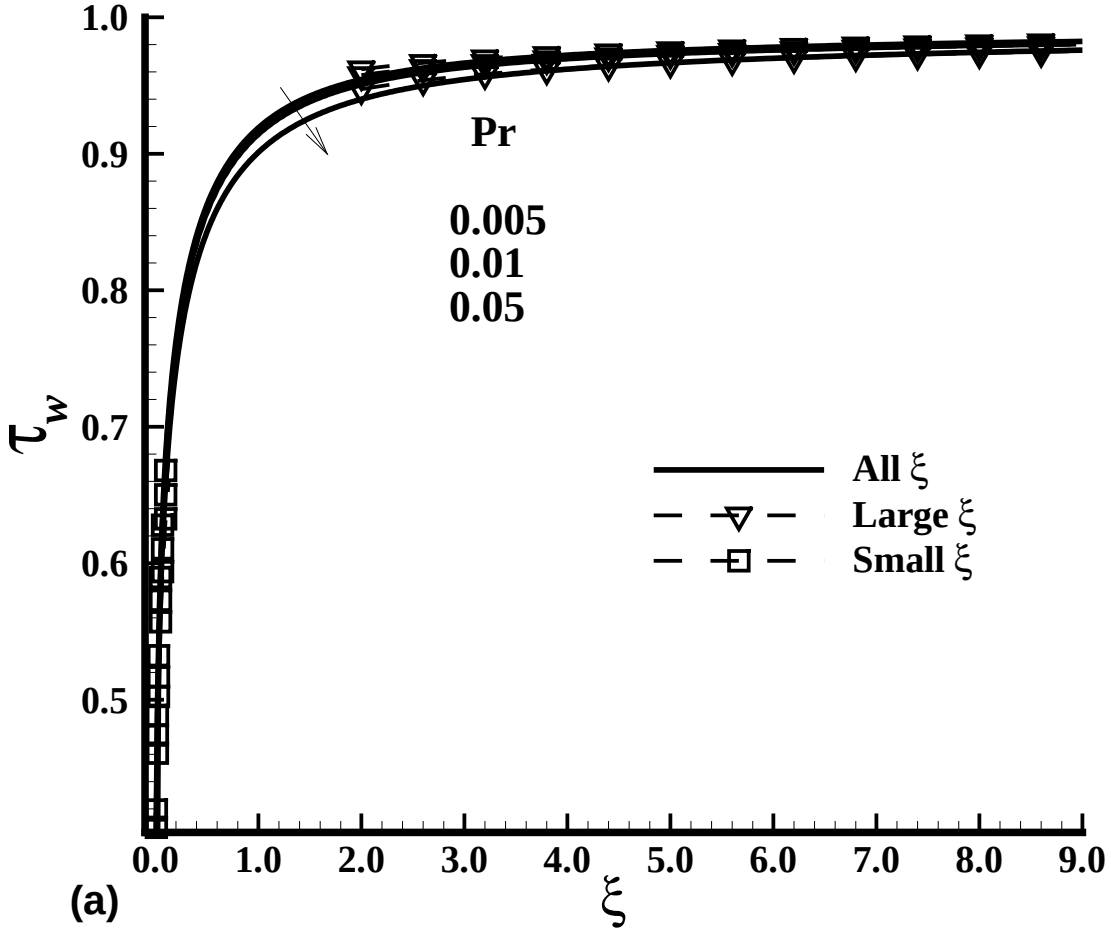

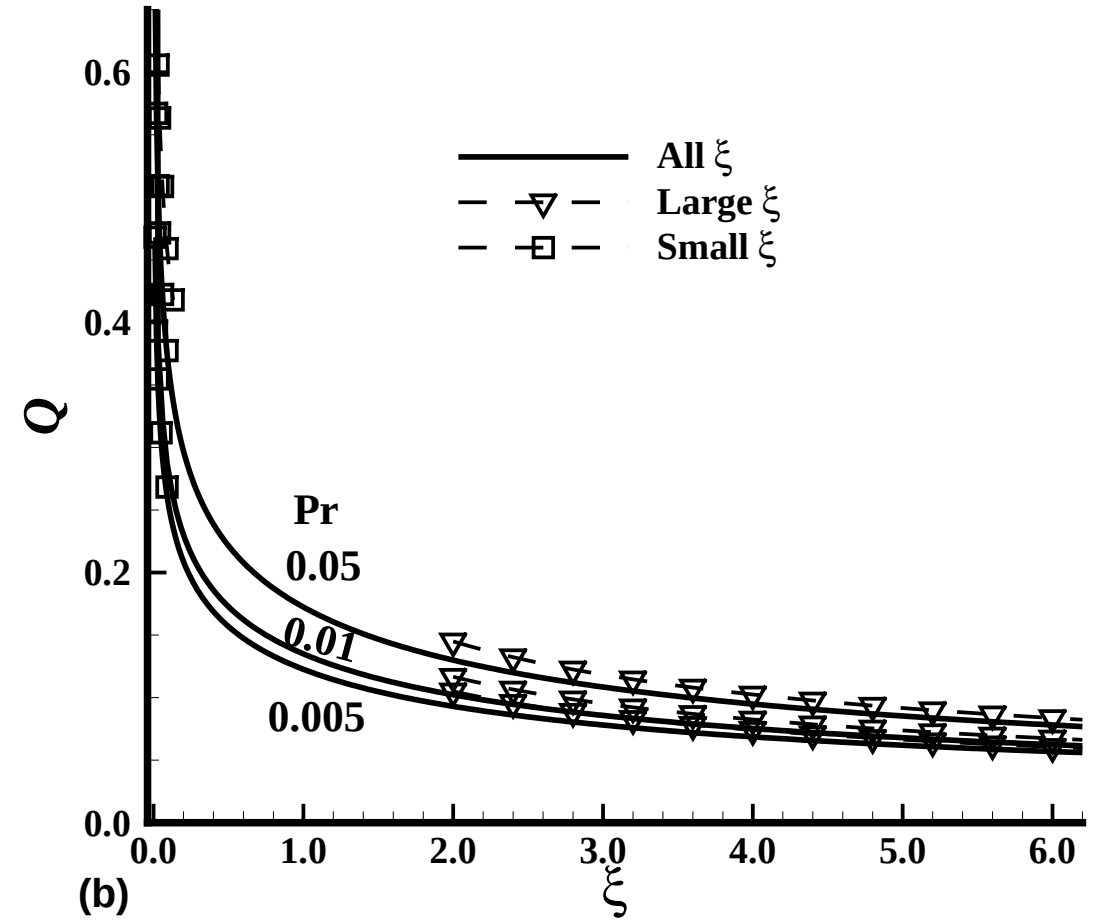

Fig. 3. (a) Variation of shear stress and (b) rate of heat transfer with ξ for Pr = 0.005, 0.01, 0.05, $R_d = 1.0$ and $\theta_w = 1.1$

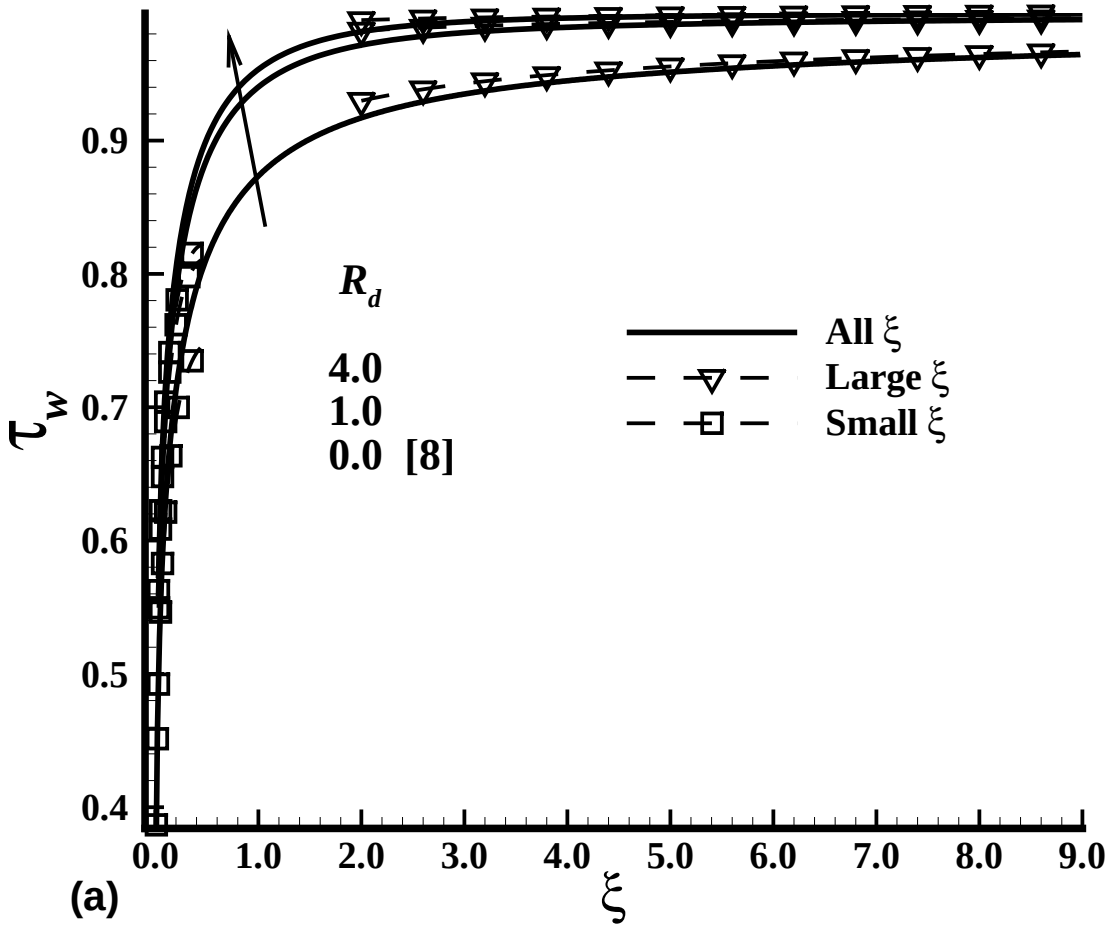

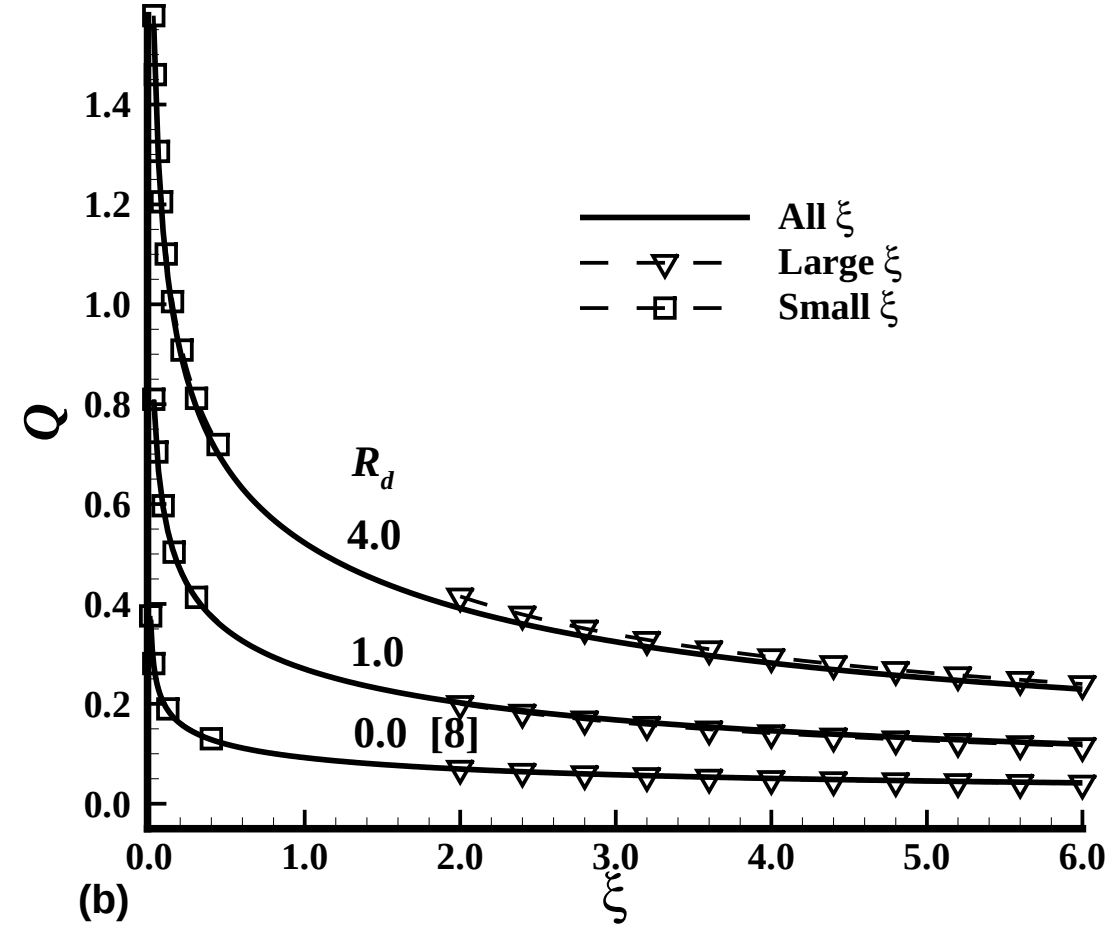

Fig. 4. (a) Variation of shear stress and (b) rate of heat transfer with ξ for $R_d = 0.0, 1.0, 4.0$ while Pr = 0.05 and $\theta_w = 2.0$

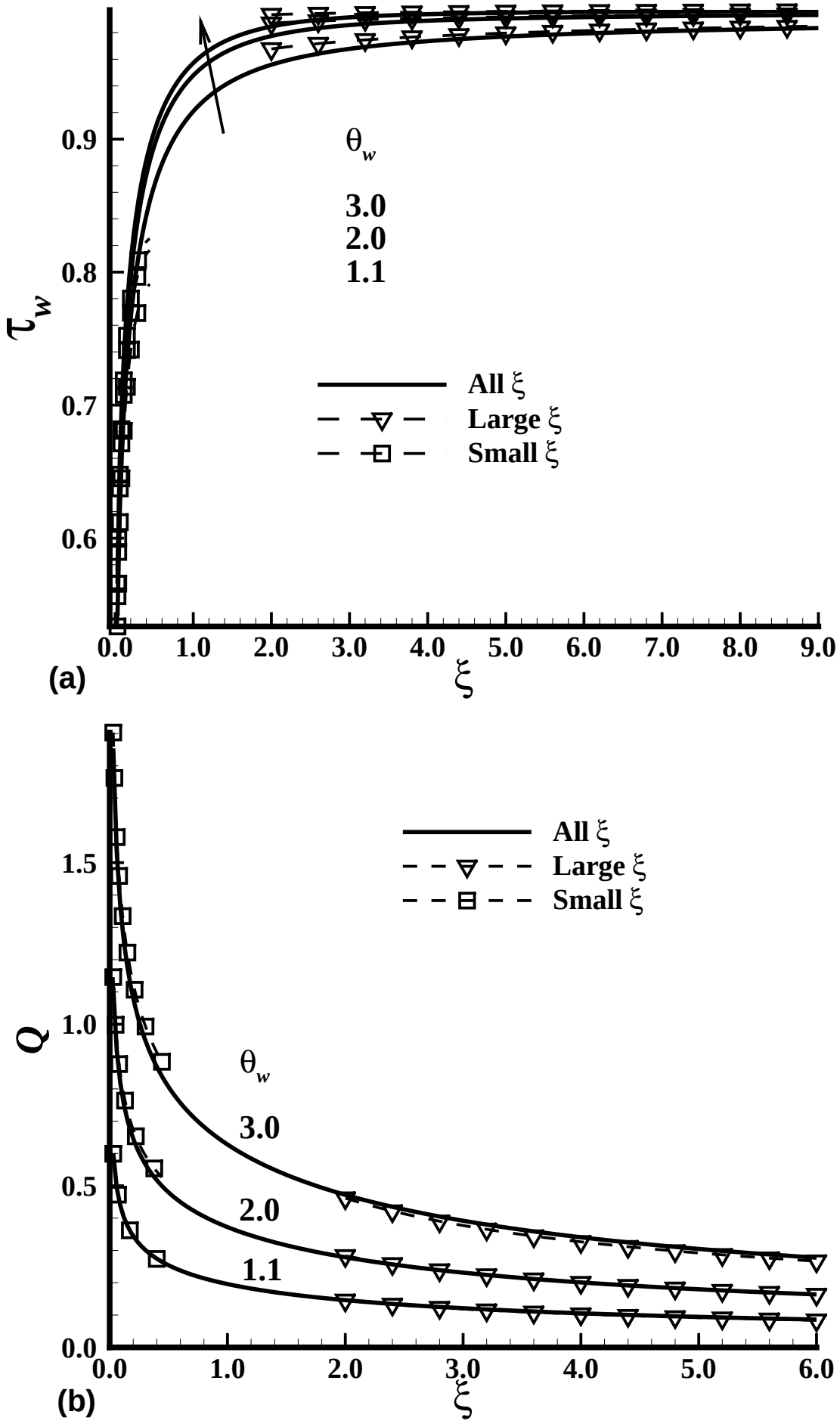

Fig. 5. (a) Variation of shear stress and (b) rate of heat transfer with ξ for $\theta_w = 1.1, 2.0, 3.0$ while Pr = 0.05 and $R_d = 2.0$

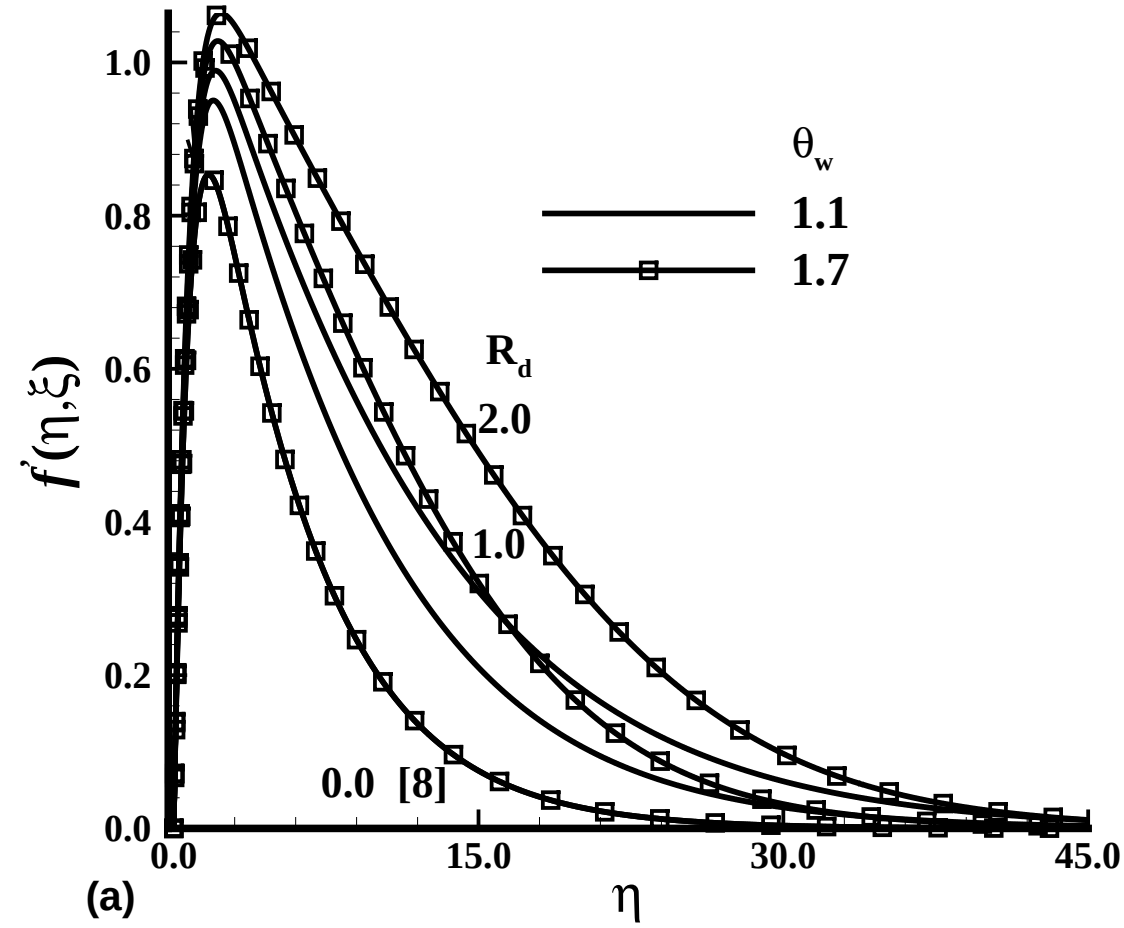

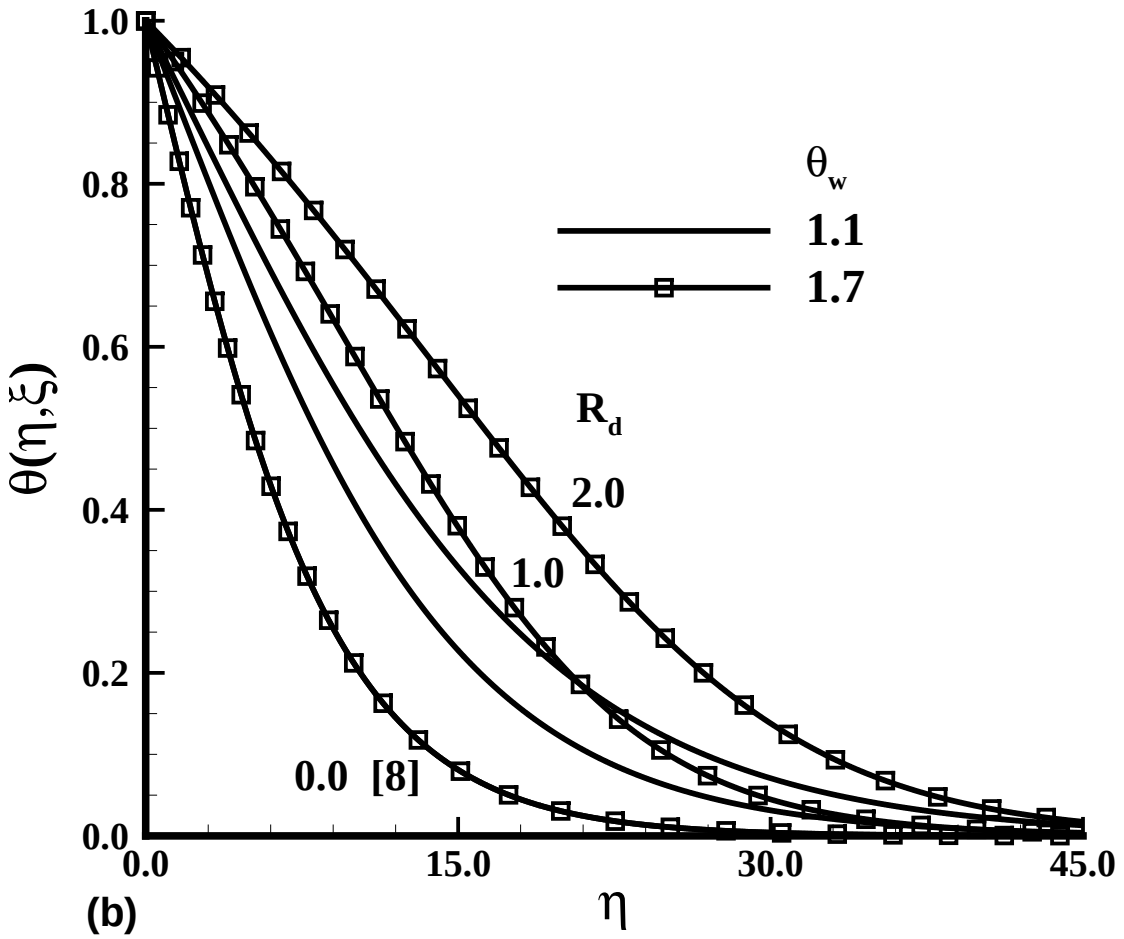

Fig. 6. (a) Velocity profile and (b) Temperature profile for $R_d = 0.0, 1.0, 2.0$ and $\theta_w = 1.1, 1.7$ while Pr=0.05 and $\xi = 1.0$

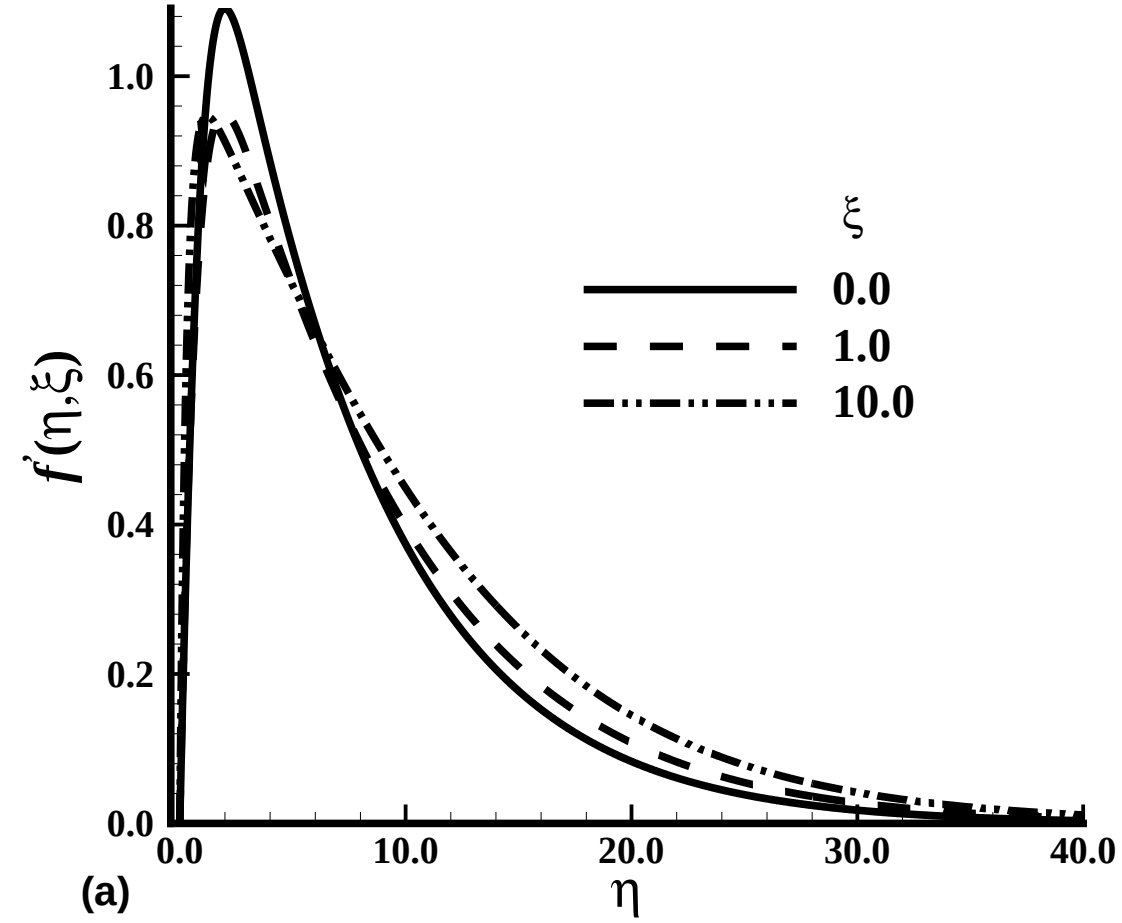

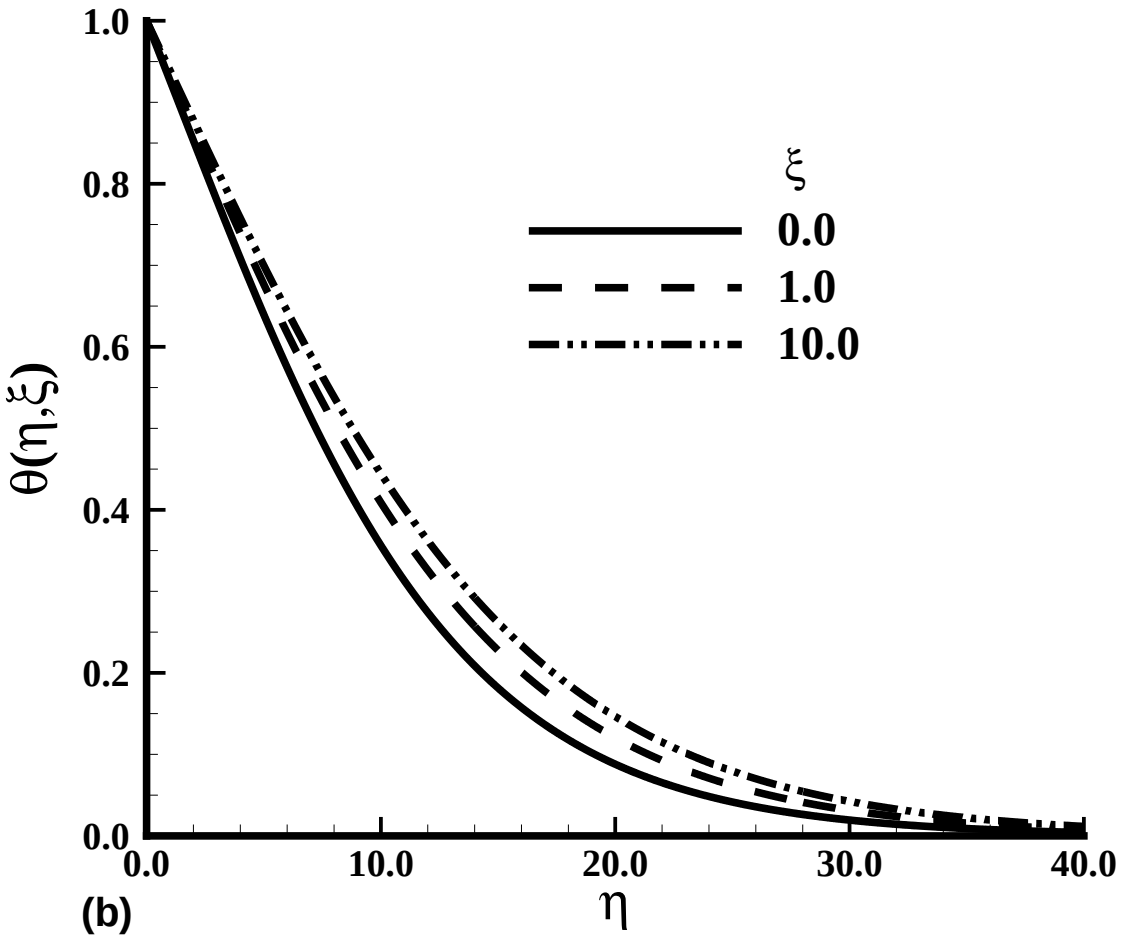

Fig. 7. (a) Velocity profile and (b) Temperature profile for $\xi = 0.0, 1.0, 10.0$ while Pr=0.05, $R_d = 1.0$ and $\theta_w = 1.1$